ACS Photonics

pubs.acs.org/journal/apchd5

Article

Spatially Structured-Mode Multiplexing Holography for High-Capacity Security Encryption

Junjie Guo, Yipeng Zhang, Hao Ye, Luyi Wang, Pengcheng Chen, Danjian Mao, Chenzhu Xie, Zhenhua Chen, Xuewei Wu, Min Xiao, and Yong Zhang*

Cite This: https://doi.org/10.1021/acsphotonics.2c01943

Read Online

ACCESS | Metrics & More | Article Recommendations

ABSTRACT: Holography has been widely used in optical displays, high-security optical encryption, and optical artificial intelligence. Optical multiplexing technologies by utilizing various dimensions of light effectively expand the information capacity and density for holography. In this work, we propose and experimentally demonstrate a novel spatially structured-mode multiplexing holography with the assistance of deep learning algorithms. In the experiment, we utilize Hermite−Gaussian (HG) and Laguerre−Gaussian (LG) modes for example as decoding channels of various holographic images. The results prove that these spatial modes work well as a multiplexing dimension in addition to wavelength, polarization, and orbital angular momentum (OAM) of light. In addition, by designing a specifically computed hologram, multiple spatial modes can be superposed together to compose a single decoding channel, which can significantly enhance the capacity and security for holographic encryption. Our work provides a promising scheme for high-capacity computational holography and information encryption.

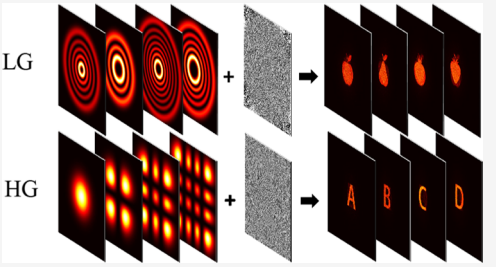

KEYWORDS: *holographic multiplexing, information encryption, spatial modes, deep learning, high capacity*

INTRODUCTION

Holography is able to reconstruct both the intensity and phase information of an object, which is of transformative potential in optical displays,[1−3] data storage,[4] information encryption,[5] and microscopy.[6] With the rapid development of digital computers, computer-generated holography (CGH) has made many important progresses in recent years. For instance, CGH has been extended from 2D to 3D using advanced optimization algorithms.[7−9] In addition to coherent light sources, partially coherent light sources are also introduced to perform optical CGH.[10] Importantly, holographic multiplexing technologies make it possible to encode multiple patterns into one hologram. In the field of optics, different physical dimensions of light have been utilized as independent information encoding/decoding channels, including wavelength,[11−13] polarization,[14−17] and orbital angular momentum (OAM).[5,18−23]

Laguerre−Gaussian (LG) modes and Hermite−Gaussian (HG) modes are the eigensolutions of a paraxial wave equation, which are capable of composing complete and orthogonal bases. LG modes feature a circular symmetry and are directly related to the OAM of photons, which play an important role in rotational Doppler shift,[24] optical image processing,[25,26] and optical communications.[27] LG modes are characterized by an azimuthal index l and a radial index p. HG modes have a rectangular symmetry and are defined by the indices of m and n along x- and y-directions, respectively. To generate high-quality HG and LG modes, many useful methods based on spatial phase modulator (SLM),[28] laser cavity,[29−31] and nonlinear optic process[32] have been proposed. The applications of these spatial modes[33−35] have recently been extended to a diffractive deep neural network.[36] Various deep learning[37] algorithms have been developed for optical recognition[38−42] and holography,[43] photonic integrated circuits,[44,45] and intelligent imaging.[46−49] Particularly, optical neural network[40,41,44,50] can accomplish challenging computer vision tasks.

In this paper, we propose the use of spatially structured modes in holographic multiplexing. In the experiment, we demonstrate two schemes. The first one is to utilize various HG (or LG) modes as multiplexing channels. The other one is to use the complex-amplitude superposition of two HG modes as multiplexing channels, which, with the assistance of a fully convolutional network, is capable of enhancing the holographic capacity and security encryption.

Received: December 12, 2022

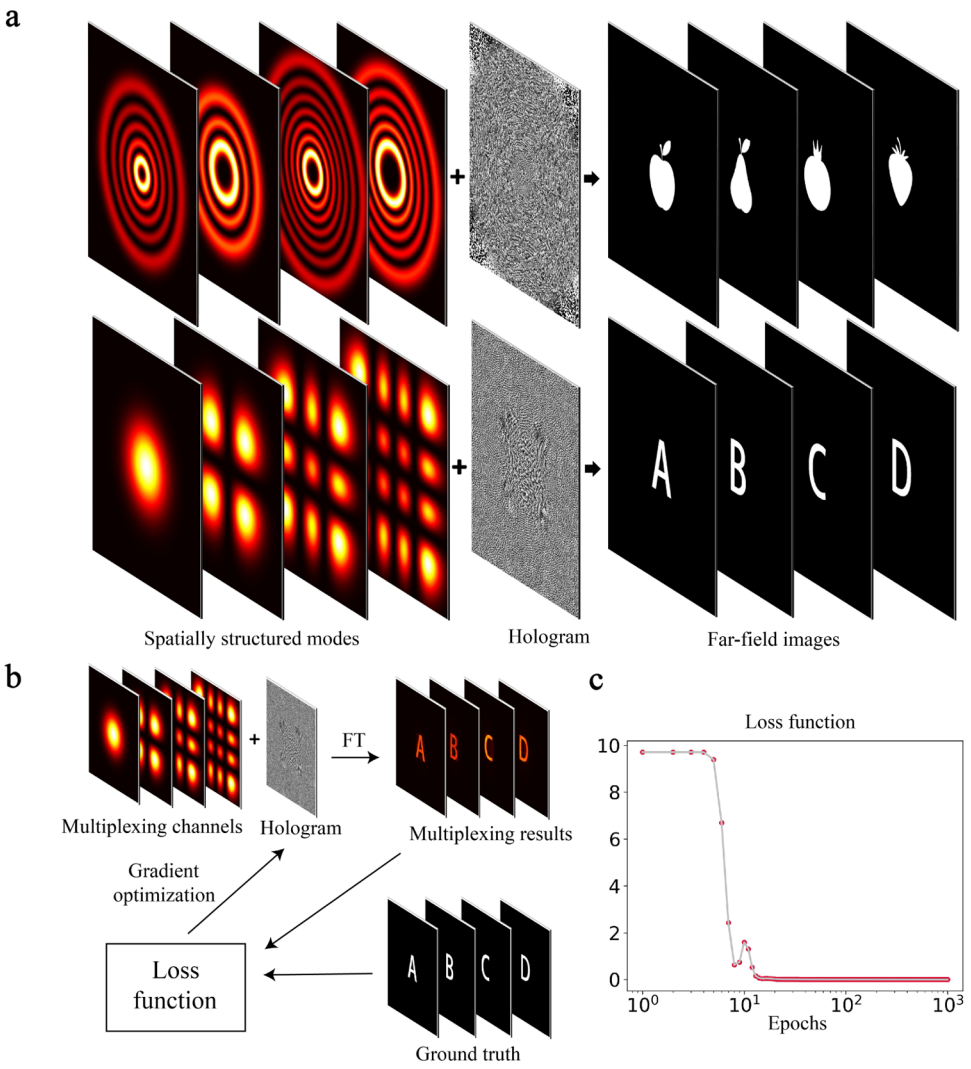

Figure 1. Principle of spatially structured-mode multiplexing holography. (a) Typical schemes based on LG and HG modes. Different images can be selectively reconstructed by choosing proper incident LG/HG modes. (b) Hologram optimization process. Here, FT represents Fourier transform. (c) Calculated loss function of four-channel HG-mode multiplexing holography, which converges to 10^{-3} after a 1000-epoch optimization process.

DESIGN PRINCIPLE

We first present the multiplexing scheme by utilizing different HG or LG modes. The design principle of spatially structured-mode multiplexing holography is illustrated in Figure 1. By inputting spatial modes of different orders (Figure 1a), one can selectively reconstruct the designed images at a far field. Figure 1b shows the algorithm to calculate the hologram. The hologram is initialized with a random phase distribution at the first epoch. Then, the output holographic images are computed after performing Fourier transform. We define the loss function as the mean square error between the output results and the ground truth (i.e., target images). Then, we adopt a gradient descent algorithm based on Adam optimizer[51] to improve the parameters of the phase hologram. During the optimization process, the learning rate is set as 1 and the number of epochs is 2000. Figure 1c shows that the loss function converges to $\sim 10^{-3}$ after 1000 epochs, which indicates the realization of spatial-mode multiplexing holography. Since our scheme is free of presampling the images, the intensity of light can be fully utilized in principle.

EXPERIMENTAL DEMONSTRATION

To experimentally demonstrate the spatial-mode multiplexing holography, we first prepare the standard HG and LG modes via SLM. According to pixelated phase computer holograms for accurate generation of scalar complex fields,[28] one can produce arbitrary spatial modes via SLM in principle. Our numerical simulations show that the generated LG and HG modes have a typical purity of >98%. Here, the SLM used in our experiment has a resolution of 1920 × 1080 pixels and a pixel size of 8 μm. In theory, one can reconstruct a certain image by inputting the corresponding spatial mode onto the phase hologram (Figure 1a). To simplify the optical alignment, we add the superposition of the decoding spatial mode and phase hologram onto SLM. Under such an experimental configuration, one can observe directly the holographic images at the first diffraction order (Figure 2a). The theoretical channel number of spatial-mode multiplexing is infinite. Here, we demonstrate four-channel multiplexing holography for example.

The optimized HG-mode and LG-mode multiplexing holograms are shown on the top of Figure 2b,2c, respectively. In the HG-mode multiplexing scheme, we choose HG(0, 0),

https://doi.org/10.1021/acsphotonics.2c01943
ACS Photonics XXXX, XXX, XXX−XXX

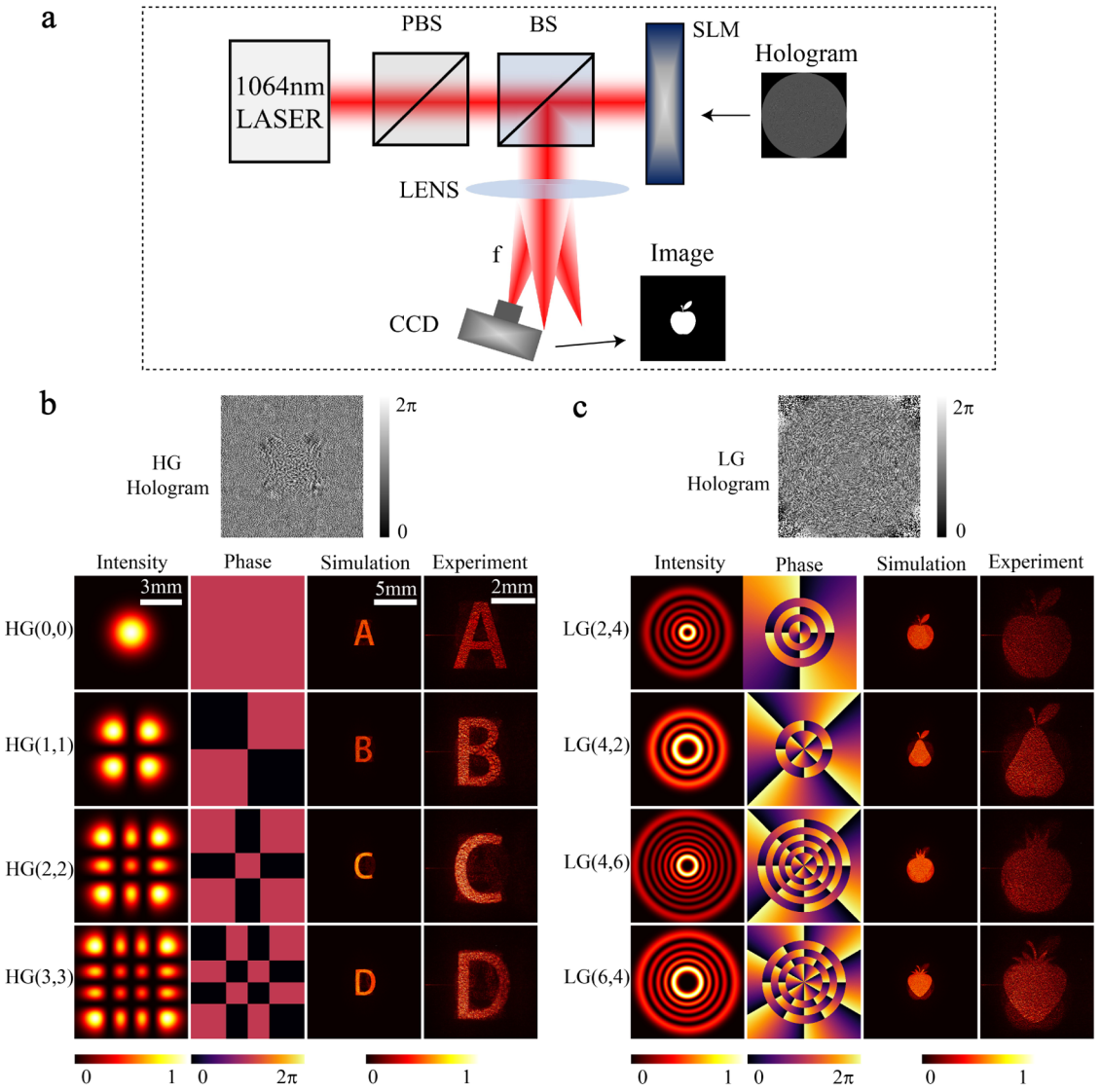

Figure 2. Experimental demonstration of holographic multiplexing based on HG and LG modes. (a) Optical setup. BS, beam splitter; PBS, polarization beam splitter; SLM, spatial light modulator. The multiplexing results are acquired at the first diffraction order by a CCD. (b, c) Optimized phase holograms. The numerical simulations and the experimental results using HG and LG modes are given under respective holograms.

HG(1, 1), HG(2, 2), and HG(3, 3) as four channels. As shown in Figure 2b, four letters "A", "B", "C", and "D" are reconstructed, respectively. Notably, it is necessary to choose those mode indices with enough spacing to suppress the crosstalk between different channels. In addition, we use four LG modes (i.e., LG(2, 4), LG(4, 2), LG(4, 6), and LG(6, 4)) to decode the images of four different fruits (Figure 2c). Clearly, both the azimuthal index l and the radial index p of LG mode can serve as effective multiplexing channels, which further expands the concept of traditional OAM-multiplexing holography. The results in Figure 2 prove that HG (or LG) modes can be designed as information channels, which works well for the construction of multiple images.

SECURITY ENCRYPTION

Next, we show that one can use the complex-amplitude superposition of two spatial modes as multiplexing channels. Here, we use HG(0, 1) and HG(1, 0) for example. In our design, these two modes and their superposition with the relative phases being 0 and π (i.e., HG(0, 1) + HG(1, 0) and HG(0, 1) + $e^{i\pi}$HG(1, 0), respectively) compose four channels. The calculated hologram is shown at the top of Figure 3a. In the experiment, numbers "1", "2", "3", and "4" are present when inputting the corresponding decoding spatial modes, which are consistent with the numerical simulations (Figure 3a). Clearly, the information can be extracted only when the input modes are superposed correctly.

In this way, one can improve the security of all-optic information encryption. Figure 3b shows a typical case. A plaintext message "121314" is encrypted as a holographic cipher text. To decrypt the information, it is necessary to input the correct HG-mode keys. Here, we define the key as (m_1, n_1, m_2, n_2, a, b), which represents spatial-mode combination of $HG(m_1, n_1) + ae^{ib\pi}\ HG(m_2, n_2)$. Then, the unique keys to reconstruct the message are (0, 1, /, /, 0, /), (1, 0, /, /, 0, /), (0, 1, /, /, 0, /), (0, 1, 1, 0, 1, 0), (0, 1, /, /, 0, /), and (0, 1, 1, 0, 1, 1). Here, the symbol "/" represents that the output is not relevant to the value of this parameter. Although there exists

https://doi.org/10.1021/acsphotonics.2c01943
ACS Photonics XXXX, XXX, XXX−XXX

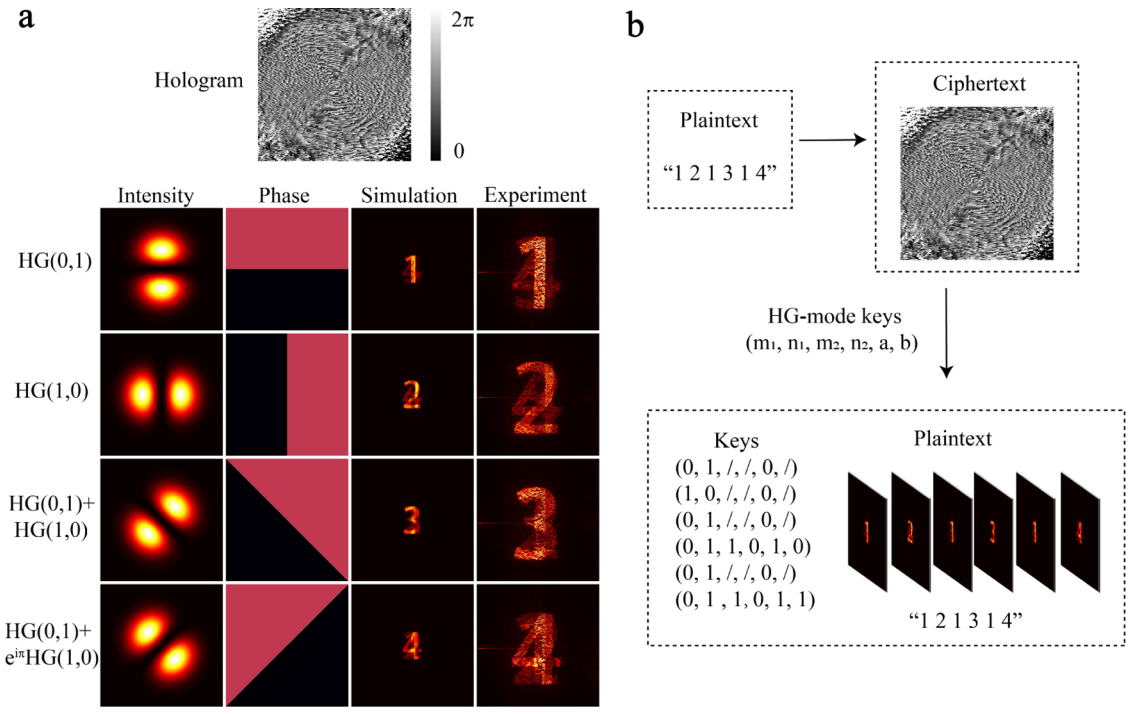

Figure 3. Holographic multiplexing through the complex-amplitude superposition of two HG modes. (a) Optimized hologram is shown at the top. In the experiment, we successfully reconstruct four numbers by inputting HG(0, 1), HG(1, 0), and the superposition of these two modes, which are well consistent with the numerical simulations. (b) Approach for security encryption. A plaintext message "121314" is encrypted as holographic cipher text, which can only be decrypted by inputting the correct six-digit keys.

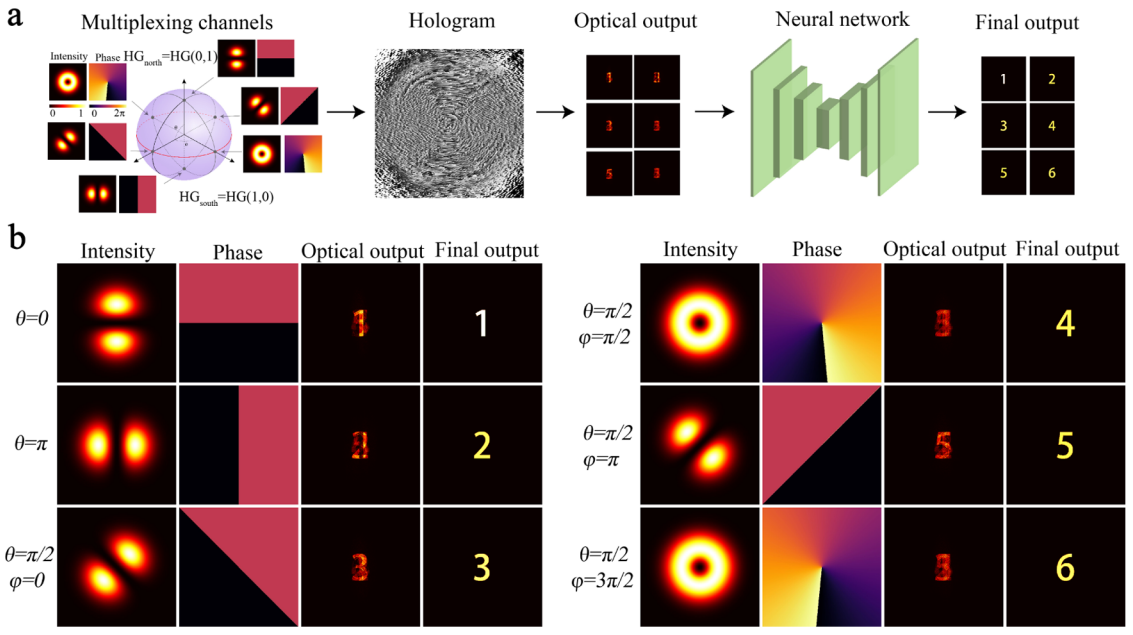

Figure 4. Holographic multiplexing using higher-order Poincare sphere modes. (a) Design principle. One can choose the spatial modes on higher-order Poincare sphere as multiplexing channels. The optical output can be further clarified by utilizing a neural network. (b) Numerical simulations show that the optical output has a certain crosstalk, which can be correctly identified through the neural network.

crosstalk between different channels, these numbers are visually distinguishable.

Such a spatial-mode-superposition multiplexing scheme can be further expanded to a higher-order Poincare sphere. As shown in Figure 4a, the north and south poles are HG(0, 1) and HG(1, 0) modes, respectively. Each point on the sphere represents a superposition with a certain relative phase and model weight, which is defined by $HG_{north}|\cos(\theta/2)| + HG_{south}|\sin(\theta/2)|\exp(i\varphi)$. Here, θ and φ define the model weight and relative phase, respectively. In theoretical design, we choose two modes at the poles and four modes at the equator as six channels for holographic multiplexing. The optimized hologram is shown in Figure 4a. When inputting different decoding modes, one can obtain six numbers from 1 to 6 separately (Figure 4b). The holography capacity can be considerably enhanced by such a spatial-mode-superposition strategy.

https://doi.org/10.1021/acsphotonics.2c01943
ACS Photonics XXXX, XXX, XXX−XXX

However, the increasing channel number induces non-negligible crosstalk (see the optical output in Figure 4b). One useful solution is to introduce an artificial neural network. Here, we design a 16-layer fully convolutional neural network to analyze the optical output and acquire the correct information (see Methods). The final output in Figure 4b is well consistent with the theoretical design, which proves the effectiveness of this approach. Clearly, one can combine the advantages of spatially structured-mode multiplexing and neural networks to build a powerful system for high-capacity information encryption.

CONCLUSIONS

In this work, we propose and experimentally realize a spatially structured-mode multiplexing scheme for high-capacity and high-security holography. HG modes, LG modes, and other spatial light modes can be utilized as information coding/decoding channels, which provide a promising dimension for optical multiplexing. Particularly, the superposition of two spatial modes can work as multiplexing channels, which provides a useful scheme to enhance the capacity of holographic encryption especially when the available spatial mode number is limited by SLMs. Such a strategy can be further extended to the superposition of multiple spatial modes. Under our current experimental condition, we have successfully realized six-channel multiplexing. Further enhancing the capacity normally requires the suppression of crosstalk between different channels by increasing the mode spacing. Another approach is to utilize neural networks including multilayer optical diffractive neural networks[18] to increase the ability to distinguish different channels, which has the potential to significantly enhance the holographic capacity and security. Our experimental results pave the way toward high-security encryption, high-capacity storage, and high-density computational holography.

METHODS

Convolutional Neural Network. In this work, the 16-layer convolutional network consists of a downsampling path and an upsampling path. The downsampling path is composed of eight convolutional layers (kernel size 4 × 4, stride 2, same padding) with nonlinear activation function (i.e., leaky rectified linear unit activation function). Note that each convolutional layer can perform twofold downsampling as well. The upsampling path has a similar structure except that the convolutional layers are replaced by the transposed convolutional layers. Both the input and output tensors of the network have a size of 1024 × 1024. In the optimization process, the learning rate is set as 10^{-3}. All our optimizations are built on tensorflow2.6[52] with Python3.9.7.

AUTHOR INFORMATION

Corresponding Author

Yong Zhang − *National Laboratory of Solid State Microstructures, College of Engineering and Applied Sciences, School of Physics, and Collaborative Innovation Center of Advanced Microstructures, Nanjing University, Nanjing 210093, China;* orcid.org/0000-0003-1158-2248; Email: zhangyong@nju.edu.cn

Authors

Junjie Guo − *National Laboratory of Solid State Microstructures, College of Engineering and Applied Sciences, School of Physics, and Collaborative Innovation Center of Advanced Microstructures, Nanjing University, Nanjing 210093, China*

Yipeng Zhang − *National Laboratory of Solid State Microstructures, College of Engineering and Applied Sciences, School of Physics, and Collaborative Innovation Center of Advanced Microstructures, Nanjing University, Nanjing 210093, China*

Hao Ye − *National Laboratory of Solid State Microstructures, College of Engineering and Applied Sciences, School of Physics, and Collaborative Innovation Center of Advanced Microstructures, Nanjing University, Nanjing 210093, China*

Luyi Wang − *National Laboratory of Solid State Microstructures, College of Engineering and Applied Sciences, School of Physics, and Collaborative Innovation Center of Advanced Microstructures, Nanjing University, Nanjing 210093, China*

Pengcheng Chen − *National Laboratory of Solid State Microstructures, College of Engineering and Applied Sciences, School of Physics, and Collaborative Innovation Center of Advanced Microstructures, Nanjing University, Nanjing 210093, China*

Danjian Mao − *National Laboratory of Solid State Microstructures, College of Engineering and Applied Sciences, School of Physics, and Collaborative Innovation Center of Advanced Microstructures, Nanjing University, Nanjing 210093, China*

Chenzhu Xie − *National Laboratory of Solid State Microstructures, College of Engineering and Applied Sciences, School of Physics, and Collaborative Innovation Center of Advanced Microstructures, Nanjing University, Nanjing 210093, China*

Zhenhua Chen − *National Laboratory of Solid State Microstructures, College of Engineering and Applied Sciences, School of Physics, and Collaborative Innovation Center of Advanced Microstructures, Nanjing University, Nanjing 210093, China*

Xuewei Wu − *National Laboratory of Solid State Microstructures, College of Engineering and Applied Sciences, School of Physics, and Collaborative Innovation Center of Advanced Microstructures, Nanjing University, Nanjing 210093, China*

Min Xiao − *National Laboratory of Solid State Microstructures, College of Engineering and Applied Sciences, School of Physics, and Collaborative Innovation Center of Advanced Microstructures, Nanjing University, Nanjing 210093, China; Department of Physics, University of Arkansas, Fayetteville, Arkansas 72701, United States*

Complete contact information is available at: https://pubs.acs.org/10.1021/acsphotonics.2c01943

Funding

The National Natural Science Foundation of China (NSFC) (91950206 and 11874213), the Fundamental Research Funds for the Central Universities (021314380220 and 021314380191), the Technology Innovation Foundation of Nanjing University (020414913416), and the GuangDong Basic and Applied Basic Research Foundation (2019A1515111128) support is acknowledged.

Notes

The authors declare no competing financial interest.

https://doi.org/10.1021/acsphotonics.2c01943
ACS Photonics XXXX, XXX, XXX−XXX

REFERENCES

(1) Blanche, P. A.; Bablumian, A.; Voorakaranam, R.; Christenson, C.; Lin, W.; Gu, T.; Flores, D.; Wang, P.; Hsieh, W. Y.; Kathaperumal, M.; Rachwal, B.; Siddiqui, O.; Thomas, J.; Norwood, R. A.; Yamamoto, M.; Peyghambarian, N. Holographic three-dimensional telepresence using large-area photorefractive polymer. *Nature* **2010**, *468*, 80−83.

(2) Makey, G.; Yavuz, Ö.; Kesim, D. K.; Turnalı, A.; Elahi, P.; Ilday, S.; Tokel, O.; Ilday, F. Ö. Breaking crosstalk limits to dynamic holography using orthogonality of high-dimensional random vectors. *Nat. Photonics* **2019**, *13*, 251−256.

(3) Zhang, S.; Huang, L.; Li, X.; Zhao, R.; Wei, Q.; Zhou, H.; Jiang, Q.; Geng, G.; Li, J.; Li, X.; Wang, Y. Dynamic Display of Full-Stokes Vectorial Holography Based on Metasurfaces. *ACS Photonics* **2021**, *8*, 1746−1753.

(4) Coufal, H. J.; Psaltis, D.; Sincerbox, G. T. *Holographic Data Storage*; Springer, 2000; Vol. *8*.

(5) Fang, X.; Ren, H.; Gu, M. Orbital angular momentum holography for high-security encryption. *Nat. Photonics* **2020**, *14*, 102−108.

(6) Alexandrov, S. A.; Hillman, T. R.; Gutzler, T.; Sampson, D. D. Synthetic Aperture Fourier Holographic Optical Microscopy. *Phys. Rev. Lett.* **2006**, *97*, No. 168102.

(7) Zhang, J.; Pégard, N.; Zhong, J.; Adesnik, H.; Waller, L. 3D computer-generated holography by non-convex optimization. *Optica* **2017**, *4*, 1306−1313.

(8) Chen, C.; Lee, B.; Li, N.-N.; Chae, M.; Wang, D.; Wang, Q.-H.; Lee, B. Multi-depth hologram generation using stochastic gradient descent algorithm with complex loss function. *Opt. Express* **2021**, *29*, 15089−15103.

(9) Jing, X.; Zhao, R.; Li, X.; Jiang, Q.; Li, C.; Geng, G.; Li, J.; Wang, Y.; Huang, L. Single-shot 3D imaging with point cloud projection based on metadevice. *Nat. Commun.* **2022**, *13*, No. 7842.

(10) Peng, Y.; Choi, S.; Kim, J.; Wetzstein, G. Speckle-free holography with partially coherent light sources and camera-in-the-loop calibration. *Sci. Adv.* **2021**, *7*, No. eabg5040.

(11) Chen, P.; Wang, C.; Wei, D.; Hu, Y.; Xu, X.; Li, J.; Wu, D.; Ma, J.; Ji, S.; Zhang, L.; Xu, L.; Wang, T.; Xu, C.; Chu, J.; Zhu, S.; Xiao, M.; Zhang, Y. Quasi-phase-matching-division multiplexing holography in a three-dimensional nonlinear photonic crystal. *Light: Sci. Appl.* **2021**, *10*, 146.

(12) Ozaki, M.; Kato, J.-i.; Kawata, S. Surface-Plasmon Holography with White-Light Illumination. *Science* **2011**, *332*, 218−220.

(13) Li, X.; Chen, L.; Li, Y.; Zhang, X.; Pu, M.; Zhao, Z.; Ma, X.; Wang, Y.; Hong, M.; Luo, X. Multicolor 3D meta-holography by broadband plasmonic modulation. *Sci. Adv.* **2016**, *2*, No. e1601102.

(14) Mueller, J. P. B.; Rubin, N. A.; Devlin, R. C.; Groever, B.; Capasso, F. Metasurface Polarization Optics: Independent Phase Control of Arbitrary Orthogonal States of Polarization. *Phys. Rev. Lett.* **2017**, *118*, No. 113901.

(15) Deng, L.; Deng, J.; Guan, Z.; Tao, J.; Chen, Y.; Yang, Y.; Zhang, D.; Tang, J.; Li, Z.; Li, Z.; Yu, S.; Zheng, G.; Xu, H.; Qiu, C.-W.; Zhang, S. Malus-metasurface-assisted polarization multiplexing. *Light: Sci. Appl.* **2020**, *9*, 101.

(16) Zhao, R.; Sain, B.; Wei, Q.; Tang, C.; Li, X.; Weiss, T.; Huang, L.; Wang, Y.; Zentgraf, T. Multichannel vectorial holographic display and encryption. *Light: Sci. Appl.* **2018**, *7*, 95.

(17) Zhao, R.; Geng, G.; Wei, Q.; Liu, Y.; Zhou, H.; Zhang, X.; He, C.; Li, X.; Li, X.; Wang, Y.; et al. Controllable Polarization and Diffraction Modulated Multi-Functionality Based on Metasurface. *Adv. Opt. Mater.* **2022**, *10*, No. 2102596.

(18) Huang, Z.; He, Y.; Wang, P.; Xiong, W.; Wu, H.; Liu, J.; Ye, H.; Li, Y.; Fan, D.; Chen, S. Orbital angular momentum deep multiplexing holography via an optical diffractive neural network. *Opt. Express* **2022**, *30*, 5569−5584.

(19) Zhou, H.; Sain, B.; Wang, Y.; Schlickriede, C.; Zhao, R.; Zhang, X.; Wei, Q.; Li, X.; Huang, L.; Zentgraf, T. Polarization-Encrypted Orbital Angular Momentum Multiplexed Metasurface Holography. *ACS Nano* **2020**, *14*, 5553−5559.

(20) Jin, L.; Huang, Y.-W.; Jin, Z.; Devlin, R. C.; Dong, Z.; Mei, S.; Jiang, M.; Chen, W. T.; Wei, Z.; Liu, H.; et al. Dielectric multi-momentum meta-transformer in the visible. *Nat. Commun.* **2019**, *10*, No. 4789.

(21) Ren, H.; Briere, G.; Fang, X.; Ni, P.; Sawant, R.; Héron, S.; Chenot, S.; Vézian, S.; Damilano, B.; Brändli, V.; et al. Metasurface orbital angular momentum holography. *Nat. Commun.* **2019**, *10*, No. 2986.

(22) Ren, H.; Fang, X.; Jang, J.; Bürger, J.; Rho, J.; Maier, S. A. Complex-amplitude metasurface-based orbital angular momentum holography in momentum space. *Nat. Nanotechnol.* **2020**, *15*, 948−955.

(23) Zhang, X.; Huang, L.; Zhao, R.; Zhou, H.; Li, X.; Geng, G.; Li, J.; Li, X.; Wang, Y.; Zhang, S. Basis function approach for diffractive pattern generation with Dammann vortex metasurfaces. *Sci. Adv.* **2022**, *8*, No. eabp8073.

(24) Allen, L.; Babiker, M.; Power, W. L. Azimuthal doppler shift in light beams with orbital angular momentum. *Opt. Commun.* **1994**, *112*, 141−144.

(25) Wei, D.; Ma, J.; Wang, T.; Xu, C.; Zhu, S.; Xiao, M.; Zhang, Y. Laguerre-Gaussian transform for rotating image processing. *Opt. Express* **2020**, *28*, 26898−26907.

(26) Ma, J.; Wei, D.; Wang, L.; Zhang, Y.; Xiao, M. High-quality reconstruction of an optical image by an efficient Laguerre-Gaussian mode decomposition method. *OSA Continuum* **2021**, *4*, 1396−1403.

(27) Wan, Z.; Shen, Y.; Wang, Z.; Shi, Z.; Liu, Q.; Fu, X. Divergence-degenerate spatial multiplexing towards future ultrahigh capacity, low error-rate optical communications. *Light: Sci. Appl.* **2022**, *11*, 144.

(28) Arrizón, V.; Ruiz, U.; Carrada, R.; González, L. A. Pixelated phase computer holograms for the accurate encoding of scalar complex fields. *J. Opt. Soc. Am. A* **2007**, *24*, 3500−3507.

(29) Naidoo, D.; Roux, F. S.; Dudley, A.; Litvin, I.; Piccirillo, B.; Marrucci, L.; Forbes, A. Controlled generation of higher-order Poincaré sphere beams from a laser. *Nat. Photonics* **2016**, *10*, 327−332.

(30) Wei, D.; Cheng, Y.; Ni, R.; Zhang, Y.; Hu, X.; Zhu, S.; Xiao, M. Generating Controllable Laguerre-Gaussian Laser Modes Through Intracavity Spin-Orbital Angular Momentum Conversion of Light. *Phys. Rev. Appl.* **2019**, *11*, No. 014038.

(31) Zhang, Y.; Wang, T.; Cheng, Y.; Wei, D.; Yao, W.; Chen, P.; Zhang, Y.; Xiao, M. Controllable laser output of high-quality cylindrical vector beam through intra-cavity mode conversion. *Appl. Phys. Lett.* **2020**, *117*, No. 111105.

(32) Zhang, Z.; Gao, Y.; Li, X.; Wang, X.; Zhao, S.; Liu, Q.; Zhao, C. Second harmonic generation of laser beams in transverse mode locking states. *Adv. Photonics* **2022**, *4*, No. 026002.

(33) Huang, Z.; Wang, P.; Liu, J.; Xiong, W.; He, Y.; Xiao, J.; Ye, H.; Li, Y.; Chen, S.; Fan, D. All-Optical Signal Processing of Vortex Beams with Diffractive Deep Neural Networks. *Phys. Rev. Appl.* **2021**, *15*, No. 014037.

(34) He, Y.; Wang, P.; Wang, C.; Liu, J.; Ye, H.; Zhou, X.; Li, Y.; Chen, S.; Zhang, X.; Fan, D. All-Optical Signal Processing in Structured Light Multiplexing with Dielectric Meta-Optics. *ACS Photonics* **2020**, *7*, 135−146.

(35) Lavery, M. P. J.; Peuntinger, C.; Günthner, K.; Banzer, P.; Elser, D.; Boyd, R. W.; Padgett, M. J.; Marquardt, C.; Leuchs, G. Free-space propagation of high-dimensional structured optical fields in an urban environment. *Sci. Adv.* **2017**, *3*, No. e1700552.

(36) Zheng, S.; Xu, S.; Fan, D. Orthogonality of diffractive deep neural network. *Opt. Lett.* **2022**, *47*, 1798−1801.

(37) LeCun, Y.; Bengio, Y.; Hinton, G. Deep learning. *Nature* **2015**, *521*, 436−444.

(38) Watanabe, S.; Shimobaba, T.; Kakue, T.; Ito, T. Hyper-parameter tuning of optical neural network classifiers for high-order Gaussian beams. *Opt. Express* **2022**, *30*, 11079−11089.

(39) Giordani, T.; Suprano, A.; Polino, E.; Acanfora, F.; Innocenti, L.; Ferraro, A.; Paternostro, M.; Spagnolo, N.; Sciarrino, F. Machine

https://doi.org/10.1021/acsphotonics.2c01943
ACS Photonics XXXX, XXX, XXX−XXX

Learning-Based Classification of Vector Vortex Beams. *Phys. Rev. Lett.* **2020**, *124*, No. 160401.
(40) Yan, T.; Wu, J.; Zhou, T.; Xie, H.; Xu, F.; Fan, J.; Fang, L.; Lin, X.; Dai, Q. Fourier-space Diffractive Deep Neural Network. *Phys. Rev. Lett.* **2019**, *123*, No. 023901.
(41) Lin, X.; Rivenson, Y.; Yardimci, N. T.; Veli, M.; Luo, Y.; Jarrahi, M.; Ozcan, A. All-optical machine learning using diffractive deep neural networks. *Science* **2018**, *361*, 1004−1008.
(42) Feng, F.; Hu, J.; Guo, Z.; Gan, J.-A.; Chen, P.-F.; Chen, G.; Min, C.; Yuan, X.; Somekh, M. Deep Learning-Enabled Orbital Angular Momentum-Based Information Encryption Transmission. *ACS Photonics* **2022**, *9*, 820−829.
(43) Wu, Y.; Ray, A.; Wei, Q.; Feizi, A.; Tong, X.; Chen, E.; Luo, Y.; Ozcan, A. Deep Learning Enables High-Throughput Analysis of Particle-Aggregation-Based Biosensors Imaged Using Holography. *ACS Photonics* **2019**, *6*, 294−301.
(44) Shen, Y.; Harris, N. C.; Skirlo, S.; Prabhu, M.; Baehr-Jones, T.; Hochberg, M.; Sun, X.; Zhao, S.; Larochelle, H.; Englund, D.; Soljačić, M. Deep learning with coherent nanophotonic circuits. *Nat. Photonics* **2017**, *11*, 441−446.
(45) Yan, T.; Yang, R.; Zheng, Z.; Lin, X.; Xiong, H.; Dai, Q. All-optical graph representation learning using integrated diffractive photonic computing units. *Sci. Adv.* **2022**, *8*, No. eabn7630.
(46) Barbastathis, G.; Ozcan, A.; Situ, G. On the use of deep learning for computational imaging. *Optica* **2019**, *6*, 921−943.
(47) Wang, F.; Bian, Y.; Wang, H.; Lyu, M.; Pedrini, G.; Osten, W.; Barbastathis, G.; Situ, G. Phase imaging with an untrained neural network. *Light: Sci. Appl.* **2020**, *9*, 77.
(48) Wang, F.; Wang, C.; Chen, M.; Gong, W.; Zhang, Y.; Han, S.; Situ, G. Far-field super-resolution ghost imaging with a deep neural network constraint. *Light: Sci. Appl.* **2022**, *11*, 1.
(49) Tseng, E.; Colburn, S.; Whitehead, J.; Huang, L.; Baek, S.-H.; Majumdar, A.; Heide, F. Neural nano-optics for high-quality thin lens imaging. *Nat. Commun.* **2021**, *12*, No. 6493.
(50) Wang, P.; Xiong, W.; Huang, Z.; He, Y.; Xie, Z.; Liu, J.; Ye, H.; Li, Y.; Fan, D.; Chen, S. Orbital angular momentum mode logical operation using optical diffractive neural network. *Photonics Res.* **2021**, *9*, 2116−2124.
(51) Kingma, D. P.; Ba, J. Adam: A method for stochastic optimization, 2014. https://arxiv.org/abs/1412.6980.
(52) Abadi, M.; Barham, P.; Chen, J.; Chen, Z.; Davis, A.; Dean, J.; Devin, M.; Ghemawat, S.; Irving, G.; Isard, M.*TensorFlow: A System for {Large-Scale} Machine Learning*, 12th USENIX Symposium on Operating Systems Design and Implementation (OSDI 16), 2016; pp 265−283.

https://doi.org/10.1021/acsphotonics.2c01943
ACS Photonics XXXX, XXX, XXX−XXX